To appear in the proceedi
of the International
Symposium on Few Body
Methods, Nanning, PRC,
4-10 August, 1985.
CONF-8508100--3

THE STUDY OF ATOMIC THREE-BODY PROBLEMS IN HYPERSPHERICAL COORDINATES

CONF-8508100--3

DE87 007920

C. D. LIN

Department of Physics, Kansas State University
Manhattan, Kansas
USA

FG02-86ER13596

ABSTRACT

The hyperspherical coordinates have been applied to study several new types of atomic and molecular problems. In this review, we will discuss the application of hyperspherical coordinates to the solution of some of the typical problems and present the new physical insights obtained from such studies. In particular, we will illustate how correlations between two excited electrons can be conveniently understood in terms of the surface harmonics at a constant hyperradius and visualized by displaying the surface charge densities on the angular coordinates that describe radial and angular correlations. It is shown that a new set of correlation quantum numbers K, T and A for any two-electron states can be deduced by analyzing the surface harmonics; here K and T describe angular correlation and A=(+1, -1 or 0) describes radial correlation. Because of the isomorphic correlations, states which have A=+1 or -1 are shown to exhibit supermultiplet structure while states which have A=0 are shown to behave like singly excited states. Therefore this classification scheme includes the independent particle approximation as a subset. The relations of these quantum numbers to the collective vibrations and rotations of molecule-like normal modes are also discussed. Applications of hyperspherical harmonics to the three-body breakup and linear triatomic collisions are also discussed briefly.

1. INTRODUCTION

Since the birth of nonrelativistic quantum theory, the independent particle approximation has been served as the basis of almost all areas of microscopic physics. In atomic, molecular and nuclear physics, the Hartree-Fock model or its equivalents have been used to explain a wealth of experimental data. Deviations from the predictions of the independent particle approximation are often treated in some form of perturbation theory.

Over the years, both physicists and chemists have been aware of the limitation of the independent particle approximation. When dealing with multi-particle excitations or scattering with three or more particles in the final state, there are fundamental difficulties in adopting the formulations based upon the independent particle approximation. These difficulties arise mostly because of the lack of a proper procedure for solving the general class of multi-particle excitations and scatterings.

In this review, we will focus on the progress made in the use of hyperspherical coordinates in solving several classes of atomic and molecular three-body problems. Particular emphasis will be given to the classification of doubly excited states of two-electron atoms where hyperspherical coordinates have been used to reveal the corrrelations of two excited electrons and to derive a set of correlation quantum numbers. Other discussions will include: (1) vibrational modes of linear triatomic molecules and collinear reactive scattering; (2) diamagnetism of atomic hydrogen. We will also mention briefly the threshold breakup of three charged particles, including electron impact ionization and proton impact ionization. The use of hyperspherical coordinates in solving these problems is responsible for our increasing understanding of these three-body systems. Several recent review articles on somewhat related works are by Fano,[1] Lin,[2] Rau[3] on two-electron atoms and by Manz[4] on molecular dynamics. More detailed references can be found in these articles. Reviews on the group theoretical approach on doubly excited states by Herrick[5] and experiments on doubly excited states of H^- by Smith[6] can be found in this volume.

We will start in Section II with a discussion of the different choices of hyperspherical coordinates and the dependence of the potential surfaces on the relative angles for several systems. In general, a hyperspherical coordinate system is defined for an N-dimensional space by retaining only one radial coordinate, with the rest the angular coordinates. In Section III, hyperspherical harmonics and the methods of solving the Schroedinger equations in hyperspherical coordinates are discussed. For bound and resonance states, we will show that a quasi-separable approximation of the hyperradial functions from other angle-dependent functions provides a first-order estimate of the full wave function. In section IV, we will address the application of hyperspherical coordinates to the classification of doubly excited states of two-electron atoms. From the analysis of the wave functions in hyperspherical coordinates a set of correlation quantum numbers are derived. These quantum numbers are then used to order the spectra of doubly excited states which exhibit new spectral regularity. Applications of hyperspherical coordinates to other three-body systems in atomic and molecular physics are then discussed in Section V. A brief summary and future perspective are given in Section VI.

2. HYPERSPHERICAL COORDINATES AND POTENTIAL SURFACES

The basic feature of hyperspherical coordinates is that there is only one radial distance which measures the size of the system under consideration; the rest of the coordinates are all angles. In principle, three of these angles are the Euler angles describing the overall rotation of the system, and the rest are angles measuring the relative orientations among the particles. In this section, we will address several different choices of hyperspherical coordinates that have been used in the literature in the calculation of special physical systems.

2.1 Doubly Excited States Of He

Historically hyperspherical coordinates were first used[7] to study the wave functions of helium atoms in the limit of $r_1 \longrightarrow 0$ and $r_2 \longrightarrow 0$. By replacing r_1 and r_2 by

$$R = (r_1^2 + r_2^2)^{1/2}$$
$$\alpha = \tan^{-1}(r_2/r_1) \qquad (1)$$

it was shown that the expansion of the ground state wave function near R=0, the Fock expansion,[8] contains terms which are powers of lnR. This was later employed by Frankowski and Pekeries[9] to show that if the Fock expansion is adopted, the variational calculation for the ground state energy of He converges much faster. The hyperspherical coordinates were used also by Wannier[10] to examine the threshold electron-impact ionization of atoms.

The renascence of applying hyperspherical coordinates to atomic three-body problems occurred after the discovery of doubly excited states of helium in 1963.[11] Fano[12] has been the crusader for promoting this approach. Although it is difficult to identify a single paper by Fano on this subject, his influence on his students and his associates is responsible for our present-day understanding of doubly excited states. The most fruitful application of hyperspherical coordinates to actual physical problems to date is probably in the area of doubly excited states of He and H^-.

There are several different ways of choosing the angles in the hyperspherical coordinate system for the two-electron atoms. We will assume the mass of the nucleus to be infinite and discuss the motion of the two electrons only. For simplicity, we will adopt[13,14] α, $\hat{r}_1$ and $\hat{r}_2$, where $\hat{r}_i$ denotes the usual spherical angles of electron i, as the five angles of our coordinate system. We can also adopt three Euler angles and two internal angles. The Euler angles describe the rotation of the whole atom, the two angles, α and θ_{12}, describe the relative orientation of the two electrons. The angle α, as defined in eq (1), measures the relative radial distances of the two electrons from the nucleus. The angular dependence of the wave function on α will be called radial correlation. The angle θ_{12} measures the angle the two electrons subtended with repect to the nucleus. The dependence of the wave function on θ_{12} will be called angular correlation. In terms of hyperspherical coordinates, the Coulomb interaction among the three charges is given by C/R where the effective charge C is

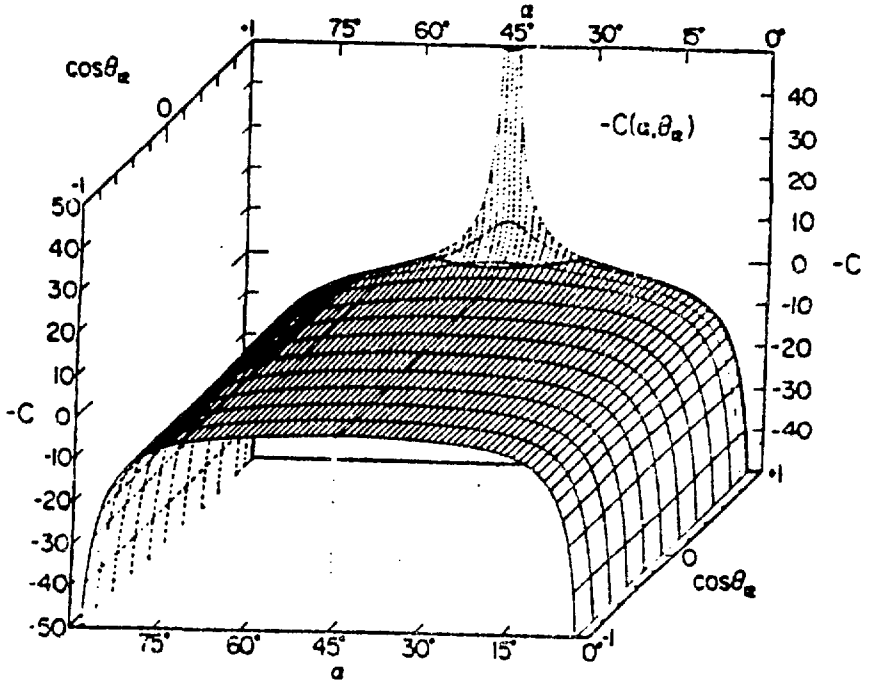

Fig. 1 The potential surface of two electrons in a Coulomb field of a nucleus of charge Z on the (α, θ_{12}) plane for Z=1 at R=1. The ordinates represent the potential in Rydbergs.

$$C = -\frac{Z}{\cos\alpha} - \frac{Z}{\sin\alpha} + \frac{1}{(1-\sin 2\alpha \cos\theta_{12})^{1/2}} \qquad (2)$$

and Z is the charge of the nucleus. In Fig. 1 we show the effective charge $C(\alpha,\theta_{12})$ on the (α,θ_{12}) plane for Z=1, or equivalently, the potential surface at R=1 for Z=1. We notice that the line along $\alpha = 45°$ is a potential ridge and there are two valleys located near $\alpha = 0°$ and $\alpha = 90°$. Each valley corresponds to the case in which one electron is near the nucleus and the other is far out. The sharp spike near $\alpha = 45°$ and $\theta_{12} = 0°$ corresponds to the two electrons being nearly on top of each other. We also point out that $\alpha = 45°$ and $\theta_{12} = 180°$ is a saddle point. This point plays an important part in the Wannier theory of threshold ionization.[15,16] It is often called the Wannier saddle point.

There are other possible choices of angles for the study of He. An alternate set was used by Klar and Klar.[17] Their coordinates are similar to the "Delves coordinates"[18] for three particles of different masses. In Delves' treatment, the coordinates are chosen democratically in that all three particles are treated on equal basis. Such a choice makes the transition from one type of system to another easier. Klar and coworkers[17] have used this democratic coordinate system to study doubly excited states and Wannier threshold law for electron impact ionization.

2.2 The H_2^+ Problem

The H_2^+ problem is traditionally treated in the Born-Oppenheimer approximation. In Fig. 2 we show the potential surface in the usual configuration space. We notice that the potential along the internuclear axis is unstable, similar to the α-coordinate in Fig. 1, while the potential along the perpendicular direction is stable, with the midpoint as the "Wannier saddle point." This aspect of the H_2^+ potential surface was emphasized by Winter and Lin[19] in the study of proton impact ionization of hydrogen atoms at low energies. A mechanism similar to the Wannier theory for electron impact ionization was emphasized to be the dominant mechanism for proton impact ionization of H at low energies.

Hyperspherical coordinates have been used by Greene[20] in an

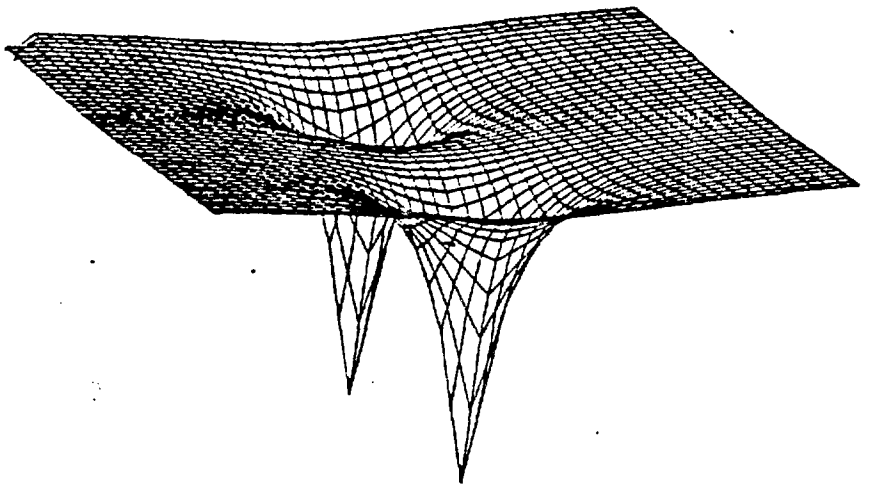

Fig. 2 The potential surface of an electron in the field of two protons. The midpoint along the internuclear axis is a saddle point.

exploratory study of the ground adiabatic potential curve of H_2^+. It was shown that the results are nearly identical to the Born-Oppenheimer adiabatic potential curve.

2.3 Collinear Triatomic Molecules

Hyperspherical coordinates have been used by quantum chemists to study the vibrational spectra and reactions of model collinear triatomic molecules in recent years. The three particles, with masses m_A, m_B, and m_C, are confined to a collinear configuration. One 'standard' coordinate system is the measure of $r_{A,BC}$, and r_{BC}. By defining

$$x = (m_{A,BC}/m)^{1/2} \; r_{A,BC} \qquad (3)$$
$$y = r_{BC}$$

where $m = m_{BC}$, the Schroedinger equation is given by

$$\left[-\frac{\hbar^2}{2m}\left(\frac{d^2}{dx^2} + \frac{d^2}{dy^2}\right) + V(x,y) - E\right] \; \Psi(x,y) = 0 \qquad (4)$$

If we define hyperspherical coordinates as

$$R = (x^2 + y^2)^{1/2} \qquad 0 \le R < \infty$$
$$\alpha = \tan^{-1}(y/x) \qquad 0 < \alpha \le \alpha_{max} \qquad (5)$$

where

$$\alpha_{max} = \tan^{-1}\left[m_B(m_A+m_B+m_C)/(m_A m_C)\right]^{1/2} \qquad (6)$$

then eq(4) becomes

$$\left[-\frac{\hbar^2}{2m}\left(\frac{1}{R}\frac{d}{dR}\left(R\frac{d}{dR}\right) + \frac{1}{R^2}\frac{d^2}{d\alpha^2}\right) + V(R,\alpha) - E\right] \; \Psi(R,\alpha) = 0 \qquad (7)$$

Equation (7) is similar to the equation describing a particle confined in a two-dimensional space (R,α). We note that the potential $V(R,\alpha)$ depends both on the radial distance as well as on the ' hyperangle ' α. As an example, consider the potential of a linear model IHI molecule.[21]

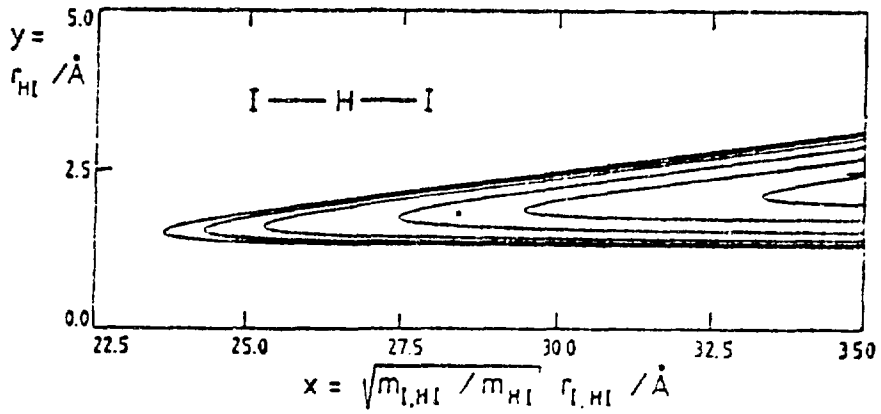

Fig. 3 Contour plots of the potential surface of a model linear triatomic IHI molecule in a mass-scaled Cartesian coordinates. (From Ref. 56.)

The potential surface is given in Fig. 3 on the (x,y) plane. The maximum angle, α_{max}, as given by eq. (6), is quite small ($\alpha_{max} = 7.2°$) for the IHI sysystem.

2.4 Quadratic Zeeman Effects

The potential surface shown in Fig. 3 is not only characteristic of a model linear triatomic molecule. In fact, if we look at the spectra of a hydrogen atom in a very strong magnetic field in the usual spherical coordinates, its potential surface is quite similar to Fig. 3. In recent years, it has been recognized[22] that a neutron star is usually surrounded by an intense magnetic field as strong as 10^8 to 10^{12} G. This strong field 'squeezes' the Bohr orbitals along the perpendicular direction such that the atomic spectroscopy is quite different from the terrestrial one. Consider a hydrogen atom in such a strong magnetic field, by choosing the z-axis along the direction of the magnetic field, the potential surface is given by

$$V(r,\theta) = -\frac{1}{r} + \frac{1}{2}\beta^2 r^2 \sin^2\theta \qquad (8)$$

where the second term is the potential energy from the quadratic Zeeman effect in appropriate units. This surface is displayed in Fig. 4. We notice that the potential at small r is dominated by the Coulomb term

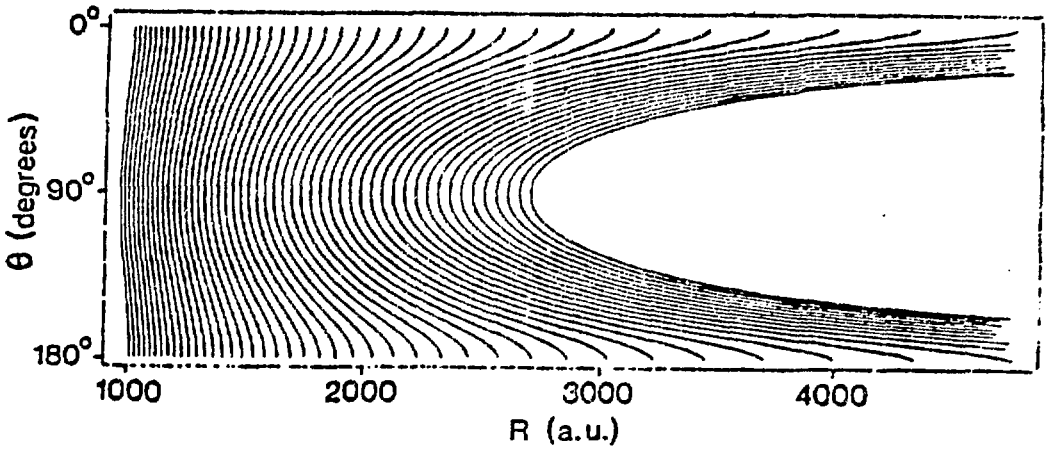

Fig. 4 Contour plot of the potential surface of a hydrogen atom in a strong magnetic field in spherical coordinates. (From Ref. 44.)

and is nearly independent of the angle θ at small r. At larger values of r, the quadratic Zeeman term dominates and the potential shows two valleys near $\theta = 0°$ and $\theta = 180°$. For a given r, the potential at $\theta = 90°$ is a maximum. This is similar to Fig. 3 where $\alpha = \alpha_{max}/2$ is also a maximum for a given R. The locus of these maxima is called a potential ridge.[23] We will see that this behavior of potential surface quite commonly occurs when many atomic and molecular systems are examined in hyperspherical coordinates. This general behavior of potential surfaces not only helps to bring about the unity of many seemingly unrelated problems, but also shows that similar theoretical approaches can be applied to different problems.

For a summary of the present section, we emphasize that the potential surfaces for a large class of atomic and molecular problems show evidence of a potential ridge and two potential valleys when expressed in hyperspherical coordinates. In the next section, we discuss the "common" theoretical approaches used to solve these problems.

3. SOLUTION OF SCHROEDINGER EQUATIONS IN HYPERSPHERICAL COORDINATES

The Schroedinger equation for each physical system can be easily expressed in hyperspherical coordinates. For the collinear triatomic molecule, for example, the IHI system, the Schroedinger equation is

given by eq. (7). For the two-electron system like He, the equation is

$$\left[-\frac{d^2}{dR^2} + \frac{\Lambda^2+15/4}{R^2} + \frac{2C}{R} - 2E\right](R^{5/2}\psi) = 0 \qquad (9)$$

where C/R is the total Coulomb interaction, with C defined in eq (2) and Λ^2 is the grand angular momentum operator, defined by

$$\Lambda^2 = -\frac{1}{\sin^2\alpha\cos^2\alpha}\frac{d}{d\alpha}(\sin^2\alpha\cos^2\alpha\frac{d}{d\alpha}) + \frac{\vec{l}_1^2}{\cos^2\alpha} + \frac{\vec{l}_2^2}{\sin^2\alpha} \qquad (10)$$

The explicit form of the grand angular momentum operator depends on the specific choice of angular coordinates. Using eq(10), the eigensolution of Λ^2 is

$$[\Lambda^2-\nu(\nu+4)]\, u_{l_1 l_2 m}(\alpha,\hat{r}_1,\hat{r}_2) = 0 \qquad (11)$$

where $\nu = l_1+l_2+2m$ and

$$u_{l_1 l_2 m} = f_{l_1 l_2 m}(\alpha)\, \mathcal{Y}_{l_1 l_2 LM}(\hat{r}_1,\hat{r}_2). \qquad (12)$$

The α-dependent function f is given by

$$f_{l_1 l_2 m}(\alpha) = N_{l_1 l_2 m}(\cos\alpha)^{l_1}(\sin\alpha)^{l_2} F(-m,m+l_1+l_2+2|l_2+\tfrac{3}{2}|\sin^2\alpha),$$

where N is a normalization constant and F is proportional to a Jacobi polynomial. The angular function

$$\mathcal{Y}_{l_1 l_2 LM}(\hat{r}_1,\hat{r}_2) = \sum_{m_1 m_2} \langle l_1 m_1 l_2 | LM\rangle\, Y_{l_1 m_1}(\hat{r}_1)\, Y_{l_2 m_2}(\hat{r}_2) \qquad (13)$$

is the coupled angular momentum function of the two electrons. The solutions in (11) are usually called hyperspherical harmonics. They are the solutions of the system in the condensation limit at R=0. A properly symmetrized hyperspherical harmonic with respect to the interchange of two electrons is given by

$$U^{SLM}_{l_1 l_2 m}(\Omega) = \frac{1}{\sqrt{2}} [f_{l_1 l_2 LM}(\alpha) \mathcal{Y}_{l_1 l_2 LM}(\hat{r}_1, \hat{r}_2) + (-1)^{l_1+l_2-L+S+m} f_{l_2 l_1 m}(\alpha)$$

$$\mathcal{Y}_{l_2 l_1 LM}(\hat{r}_1, \hat{r}_2)] \qquad \text{if } l_1 \neq l_2$$

$$= \frac{1}{2} [1 + (-1)^{-L+S+m}] f_{11m}(\alpha) \mathcal{Y}_{11LM}(\hat{r}_1, \hat{r}_2) \qquad \text{if } l_1 = l_2 = 1. \tag{14}$$

In the early application of hyperspherical coordinates, the wave functions are usually expanded in the form[23]

$$\Psi(\vec{r}_1, \vec{r}_2) = \sum_{l_1 l_2 m} F_{l_1 l_2 m}(R) \; U_{l_1 l_2 m}(\Omega) \tag{15}$$

where the functions $U_{l_1 l_2 m}$ are the hyperspherical harmonics (14) of the given problem. This expansion allows one to reduce the partial differential equation such as (7) or (9) to a system of coupled ordinary differential equations. This approach has been used in several studies of atomic[24] and nuclear[25] problems, where the expansion has been truncated to a limited number of terms. The method turns out to be not very useful since the asymptotic region is not well represented by only a few terms of hyperspherical harmonics and thus (15) converges very slowly.

The great progress made in the last few years in the application of hyperspherical coordinates in atomic and molecular problems lies in the recognition that the Schroedinger equation can be solved using a quasi-separable approximation.[13] We will write down the explicit expression for the two-electron case below. By denoting all the angles collectively as $\Omega = (\alpha, \hat{r}_1, \hat{r}_2)$, we expand the total wave function as

$$\Psi^n_\mu(R, \Omega) = \sum_\mu F^n_\mu(R) \Phi_\mu(R; \Omega) / (R^{5/2} \sin\alpha\cos\alpha) \tag{16}$$

where μ identifies the 'channel', and n denotes the n-th state within that channel. The channel function satisfies the differential equation

$$\frac{1}{R^2}\left[\frac{d^2}{d\alpha^2} + \frac{\vec{l}_1^2}{\cos^2\alpha} + \frac{\vec{l}_2^2}{\sin^2\alpha} + 2RC\right] \Phi_\mu(R;\Omega) = U_\mu(R)\Phi_\mu(R;\Omega) \qquad (17)$$

and the hyperradial function F(R) satisfies the coupled equations,

$$\left[\frac{d^2}{dR^2} + \frac{1/4}{R^2} - U_\mu(R)+W_{\mu\mu}(R)+2E_n\right] F^n_\mu(R)+ \sum_\nu W_{\mu\nu}(R)F^n_\nu(R)=0 \qquad (18)$$

where the coupling terms $W_{\mu\nu}(R)$ are defined as

$$W_{\mu\nu} = 2\langle\Phi_\mu \left|\frac{d}{dR}\right| \Phi_\nu\rangle \frac{d}{dR} + \langle\Phi_\mu\left|\frac{d^2}{dR^2}\right| \Phi_\nu\rangle \qquad (19)$$

By dropping the channel couplings and keeping all the diagonal terms, eq. (18) reduces to

$$\left[\frac{d^2}{dR^2} + \frac{1/4}{R^2} - U_\mu(R)+W_{\mu\mu}(R)+2E_n\right] F^n_\mu(R)=0 \qquad (18')$$

This equation allows for an estimate of the energy of a given state for a given channel. The potential curve $U_\mu(R)$ and the channel function serve to identify the important physics for all the states belonging to that channel.

4. DOUBLY EXCITED STATES OF HE AND H^-

In this section we will illustrate the solution of two-electron atoms in hyperspherical coordinates in the quasi-separable approximation. The method is applied to study the Feshbach and shape resonances of H^-. It is then applied to doubly excited states of He where we discuss: (1) the analysis of channel function to extract approximate quantum numbers for describing correlations of the two electrons; (2) the existence of supermultiplet structure of the energy levels of doubly excited states; and (3) the analysis of correlation quantum numbers in the body frame of the atom.

4.1 Solution Of The Channel Functions

The partial differential equation (17) for the channel functions Φ_μ and channel potentials $U_\mu(R)$ can be solved by various methods.[13,14,26,27] One straight-forward approach is to diagonalize the equation using the hyperspherical harmonic basis.[14] This method is relatively easy to do, but the convergence of the method is not very satisfactory at large R when the state is confined to one of the potential valleys. This is because the asymptotic solution is a linear combination of hydrogenic functions which is not easily expanded in terms of hyperspherical harmonics. One of the more efficient method is to employ some set of analytical basis functions which approach the large R limits correctly.[27] Together with the hyperspherical harmonics, these basis functions are used to diagonalize eq (17) to obtain the potential curves $U_\mu(R)$ and the channel functions. This method was found to be quite efficient and only a small basis set is needed.

4.2 Feshbach and Shape Resonances In H^-[28]

The potential curves for different L, S and π can be calculated using the method mentioned above. In Fig. 5, we show the three potential curves for $^1P^o$ symmetry of H^- that converge to the N=2 limit of H. The two lowest curves cross at R = 13.5 a.u. The origin of such a crossing will be discussed later. For the moment, we note that the curve designated as "+" has an attractive potential well at small R, but it has a repulsive potential barrier at large R. A potential which has this shape usually gives shape resonances. This is indeed the case. By solving the one-dimensional hyperradial equation (18') with such a potential, a shape resonance with energy 32 meV above the threshold and width 28 meV was obtained. Experimentally this resonance has been observed in electron-hydrogen atom scattering,[29] but the most elegant data were taken by Bryant et al.[30] through the photodetachment of H^-. The lack of a suitable intense light source in the desired energy region (>12.6eV) made experiments with lasers or synchrotron radiation impossible. Bryant et al. solved this problem by using the 800 MeV (v/c=0.83) relativistic H^- beam from the LAMPF facility at

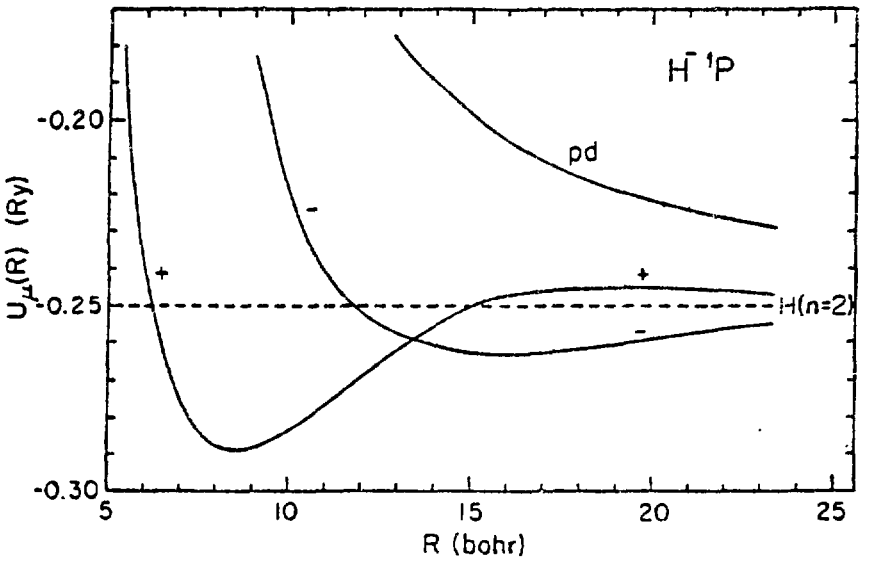

Fig. 5 Effective potential curves for the three $^1P^o$ channels of H^- that converge to the hydrogenic N=2 limit.

Los Almos, by intercepting the H^- beam upstream with a laser. By adjusting the incident angle of the laser beam, the laser is blue-shifted to the desired energy range in the H^- frame. The result of their experiment is shown in Fig. 6. The shape resonance was found to have a width of 23±6 meV. The calculated results quoted above are in reasonable agreement with these data. In Fig. 6 we also notice that there is a very narrow resonance lying below the N=2 limit at photon energy of 10.95ev. This type of resonance is called a Feshbach resonance and is quite common in atomic physics. This resonance belongs to the "-" channel and can be calculated from the "-" potential curve of Fig. 5. The result of such a calculation gives an energy 26 meV below the N=2 limit. The separation between the shape and the Feshbach resonances was measured to be 53 meV, which is to be compared with the value of 58 meV obtained from the simple calculation using quasi-separable approximation in hyperspherical coordinates.

It is interesting to mention that the shape resonance discussed above is the only known shape resonance in H^-; all the rest are Feshbach resonances. Historically when resonances were first observed in e-H scattering, they were interpreted to be shape resonances. It

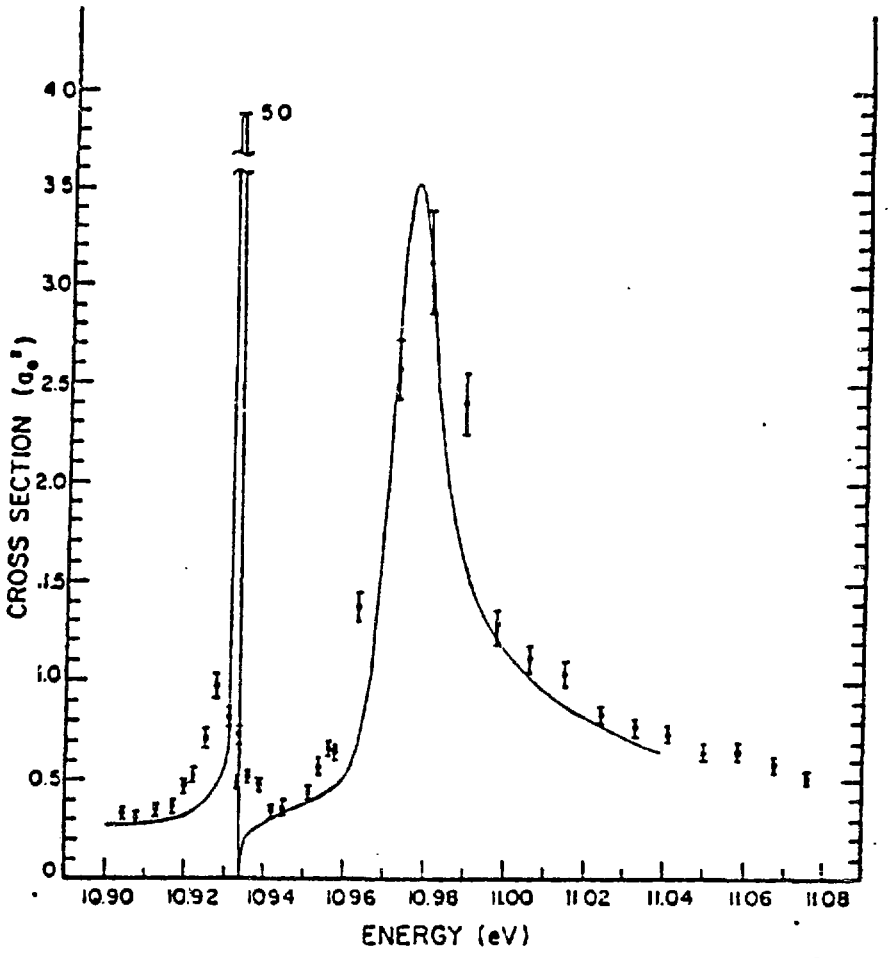

Fig. 6 Photodetachment cross sections of H^- near the N=2 excitation threshold of H. Experimental data are from Ref. 30 and the solid line represents the calculation of Broad and Reinhardt (Ref. 57).

took several years until close-coupling calculations showed that most of these resonances were Feshbach resonances.

4.3 Isomorphic Potential Curves and Isomorphic Correlations[31,32]

The greatest contribution of the use of hyperspherical coordinates in atomic physics so far is probably in the classification of doubly excited states. In Fig. 7 we show the potential curves for $^{1,3}S^e$, $^{1,3}P^o$, $^{1,3}D^e$ of He that converge to the N=3 limit of He^+. The curves are labelled with quantum numbers which will be explained later. One first notices that the curves that have been labelled with identical

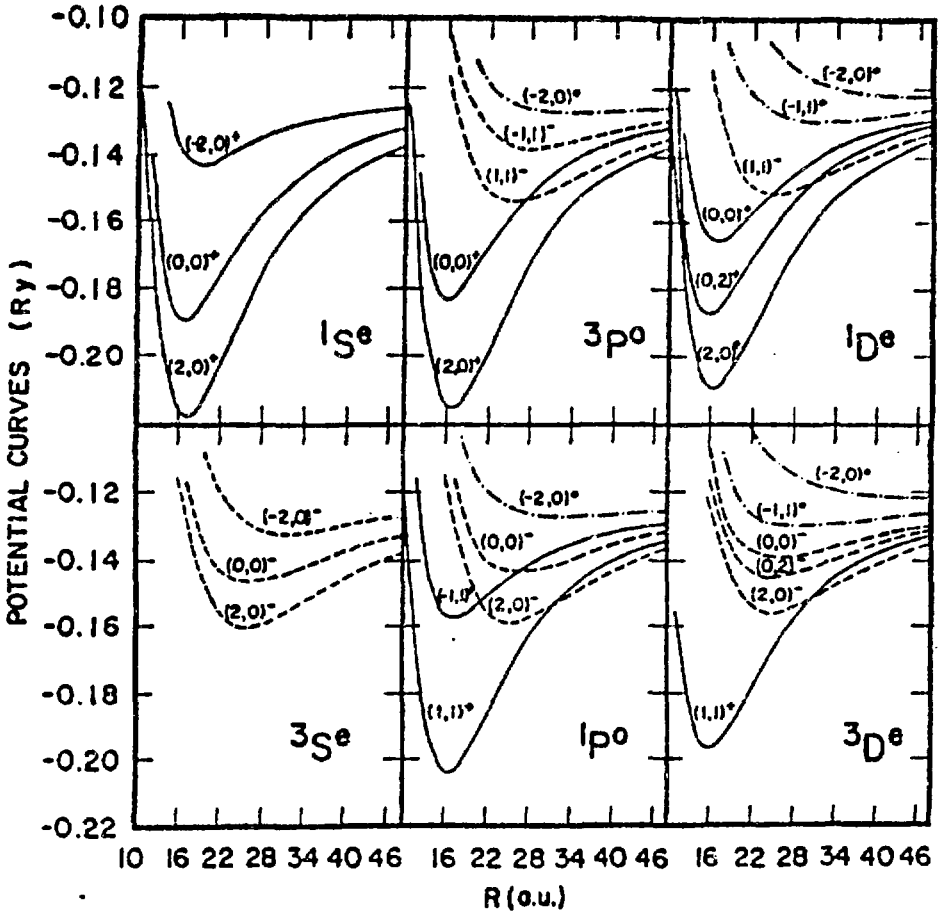

Fig. 7 Effective potential curves for the $^{1,3}S^e$, $^{1,3}P^o$ and $^{1,3}D^e$ channels of He that converge to the N=3 limit of He^+. Curves are labelled in terms of correlation quantum numbers K, T and A. Reduced units with Z=1 are used.

quantum numbers are quite similar in shape and in values. To understand this quasi-degeneracy, we have to examine the channel functions.

The channel functions Φ_μ in the quasi-separable approximation evolve smoothly from the small R region to the large R region. We first examine the channel function in the large R limit. In this asymptotic limit, one electron is moving far outside and the other stays inside, corresponding to the limit of $\alpha \to 0$ and $R \to \infty$, and the wave function is represented by the product of two independent-electron functions. In this limit, it is easier to transform eq (16) to the

independent particle coordinates, $r_2 = R\sin\alpha$, $r_1 = R\cos\alpha = R$ where the asymptotic potential for the outer electron is

$$V_\alpha(r_1) = \frac{2r_2}{r_1^2}\cos\theta_{12} + \frac{\vec{l}_1^2}{r_1^2} \qquad (20)$$

In the traditional dipole approximation,[33] the potential (20) is diagonalized within a given hydrogenic N-manifold and the channel is represented by the eigenvalues of (20). This does not provide a set of convenient quantum numbers for labelling the channels in the asymptotic limit. A more convenient approximate basis was introduced by Herrick.[34] In this 'zero-order dipole basis', only the dipole term $2r_2\cos\theta_{12}/r_1^2$ of (20) is diagonalized. In this basis, each channel for a given N, L is characterized by two quantum numbers, K and T. The eigenvalue of $r_2\cos\theta_{12}$ in this $|NKTL\rangle$ representation is

$$\langle NKTL|r_2\cos\theta_{12}|NKTL\rangle = -3NK/Z \qquad (21)$$

We notice that this zero-order dipole operator is degenerate with respect to T. This degeneracy is removed when the centrifugal potential $\vec{l}_1^2$ is included in a perturbation calculation. In a perturbative calculation, Herrick[34] has shown that the dipole potential in the asymptotic limit is given by α_d/r_1^2 with

$$\alpha_d = -3NK/Z + L(L+1) + \frac{1}{2}(N^2-1-K^2-3T^2)$$

$$-(KZ/12N)\,[8L(L+1)+N^2-1-K^2-15T^2] + \ldots \qquad (22)$$

in the $|NKTL\rangle$ basis space.

Equation (22) provides the basis of labelling the channels in the asymptotic region. Accordingly, the effective dipole potential is most attractive for large K and for a given K, for large T. Since K is proportional to $\cos\theta_{12}$, it gives information on angular correlations only. No information on radial correlations is provided.

From the potential surface shown in Fig. 1, it is evident that the potential surface does not depend very much on the angle θ_{12}. We thus expect that the dependence of the channel function on θ_{12} does not vary significantly with R. This has been proved also from the result of numerical calculations.[35] We thus expect to use K and T quantum numbers to label angular correlations in the whole range of R. To account for radial correlations, a new radial correlation quantum number A was introduced. The only values assigned to A were +1, -1 and 0.

The value of A was first assigned semi-empirically by examining the wave functions in the angle α. There are channels which are similar to $^1s^e$ states which exhibit an antinode at $\alpha = 45°$, while there are others which have a node at $\alpha = 45°$; the former are assigned to have A=+1 and the latter A=-1. There are still other channels where the electrons are always confined in the potential valleys. For these channels, the electrons never reach the plateau region (see Fig. 1) along $\alpha = 45°$; these channels are assigned A=0. All the singly excited states are assigned to have A=0.

The quantum numbers K, T and A described above can be obtained from the following rules:[36]

$$\begin{aligned} &T=0,\ 1,\ 2,\ \ldots\ldots\ldots\ldots,\min(L,N-1) \\ &K=N-1-T,\ N-3-T,\ \ldots\ldots\ldots,\ -(N-1-T) \end{aligned} \tag{23}$$

where T=0 is not allowed if $\pi = (-1)^{L+1}$. For the radial correlation quantum number A, an empirical rule is:[37]

$$\begin{aligned} &A = \pi(-1)^{S+T} = \pi(-1)^{S+N-K+1} && \text{if } K > L-N \\ &A = 0 && \text{if } K \leq L-N \end{aligned} \tag{24}$$

These two equations allow us to enumerate all the possible combinations of allowable $(K,T)^A$ labels. An alternative derivation of the quantum numbers T and A will be given in subsection (4.5). For the moment we discuss the consequence of this new classification scheme.

Referring back to Fig. 7, we notice that channels which have been assigned for the same quantum numbers have nearly identical shape and values. In connecting the diabatic curves, we first assign K and T quantum numbers to each curve in the asymptotic region, with the larger K to the lower curve and for a given K, the larger T to the lower curve. In this outer region, the value of A does not matter. In the inner region, the lower or more attractive curves belong to the A=+1 channels. Among the '+' channels, the larger K goes with the lower curve and for a given K, the larger T with the lower curve. First all the A=+1 curves are assigned, then the A=-1 channels, and last the A=0 using the same rule for each A group. By connecting channels in the two regions for curves with identical K and T, the potential curves shown in Fig. 7 are obtained. Notice that only + and - channels cross. These crossings are due to the fact that radial correlations are more important than angular correlations at small R while at large R only angular correlations are important.

4.4 Isomorphic Correlations

Two important consequences resulting from the assignment of correlation quantum numbers are: (1) Isomorphic correlations of channels with identical $(K,T)^A$ quantum numbers; (2) Supermultiplet structure for levels with identical correlation quantum numbers. In the remainder of this subsection, we discuss the isomorphism.

In Fig. 8 we display the surface charge densities of the $(2,0)^+$ channels of the $^1S^e$, $^3P^o$, $^1D^e$, and $^3F^o$ symmetries of He below $He^+(N=3)$ at R=20 a.u. We notice that the correlation patterns for all these channels are very similar despite that the L, S and π are different. At $\theta_{12}=180°$, all these channels have large charge densities which are characteristic of channels with the largest allowed K=N-1 for the given N-manifold. The charge density also peaks along $\alpha = 45°$ for any value of θ_{12}. The $\alpha = 45°$ line is an antinodal line. This is consistent with the assignment of A=+1 for all these channels.

In Fig. 9 we display the surface charge densities of the $(1,1)^+$ $^1P^o$, $(1,1)^+$ $^3D^e$, $(1,1)^-$ $^3P^o$ and $(1,1)^-$ $^1D^e$ channels of He at the R values indicated. We note here that the angle between the two

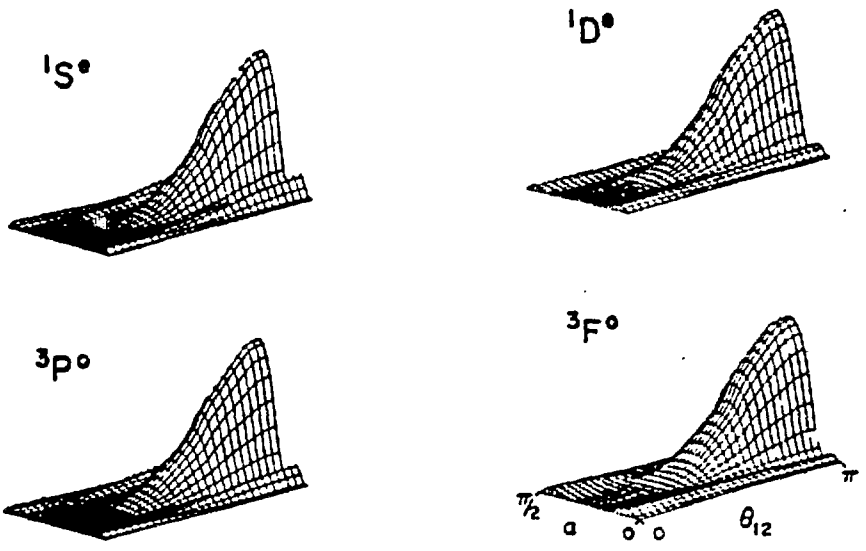

Fig. 8 Surface charge densities for the $(2,0)^+$ channel of $^1S^e$, $^3P^o$, $^1D^e$, and $^3F^o$ of He at R=20 bohrs.

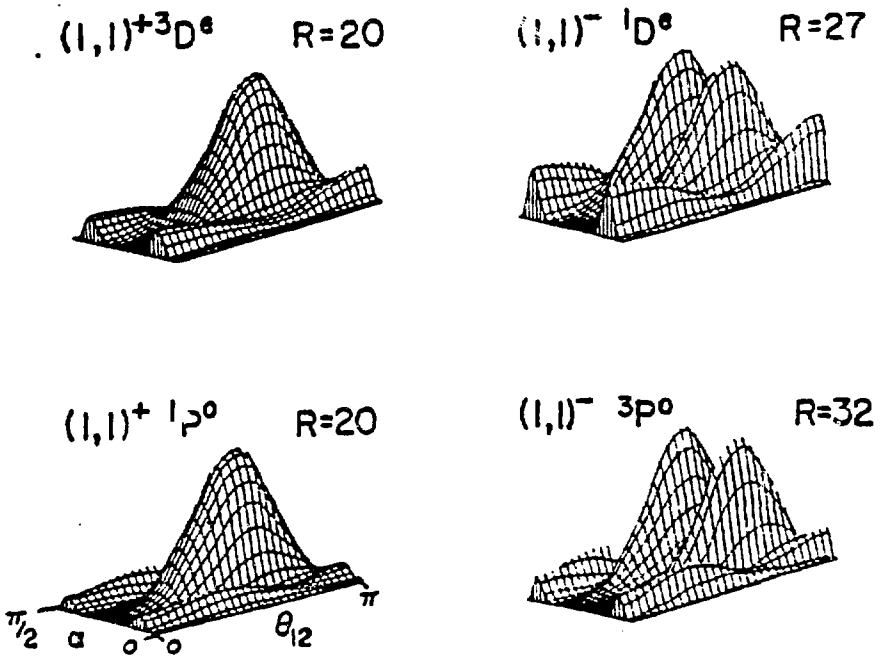

Fig. 9 Same as Fig. 8 except for the $(1,1)^+$ and $(1,1)^-$ channels shown.

electrons, θ_{12}, tends to stay near 120° and that the nodal structure near $\alpha = 45°$ for each channel is consistent with the + or - values of A assigned for that channel.

4.5 Supermultiplet Structure

In Fig. 7 we gave an example which shows that potential curves labelled by the same correlation quantum numbers K, T and A are nearly identical. Under the quasi-separable approximation, the energy levels for a given channel are obtained by solving the one-dimensional hyperradial equation (18'). Since the potentials with identical $(K,T)^A$ designations are nearly degenerate, we expect that the energy levels of these channels are also nearly degenerate. Thus by grouping the energy levels according to the correlation quantum numbers, a regular rotor structure is observed. This behavior was first discovered by Herrick and coworkers[38] for intrashell doubly excited states and examined by Berry and coworkers[39] in their model study of the spectrum of two electrons on a spherical surface.

In Fig. 10 we plot the effective principal quantum numbers n* of helium doubly excited states below the He^+ (N=3) limits for the first few low-lying states vs the correlation quantum numbers $(K,T)^A$. The + and - groups are displayed separately. Two spectral regularities are evident:

(1) The existence of rotorlike structure for states which have the same (K,T) but different L, S and π. The string of each rotor series is determined by the possible values of L, S and π which give the required $(K,T)^A$ [see eqs. (23) and (24)]. The larger the value of N is, the longer is the string. In fact, for a given K, T and N, the allowed range of L for a rotor series is L=T, T+1,....., K+N-1. Whether the rotor series is + or - is governed by eq.(24).

(2) There is a repetition of the $(K,T)^+$ and $(K,T)^-$ rotor structure. This is not surprising in view of eqs. 23 and 24. Note that the allowed K and T do not depend on the spin. A $(K,T)^+$ channel for spin singlet(triplet) becomes a $(K,T)^-$ channel for spin tripelt(singlet) with fixed L and π.

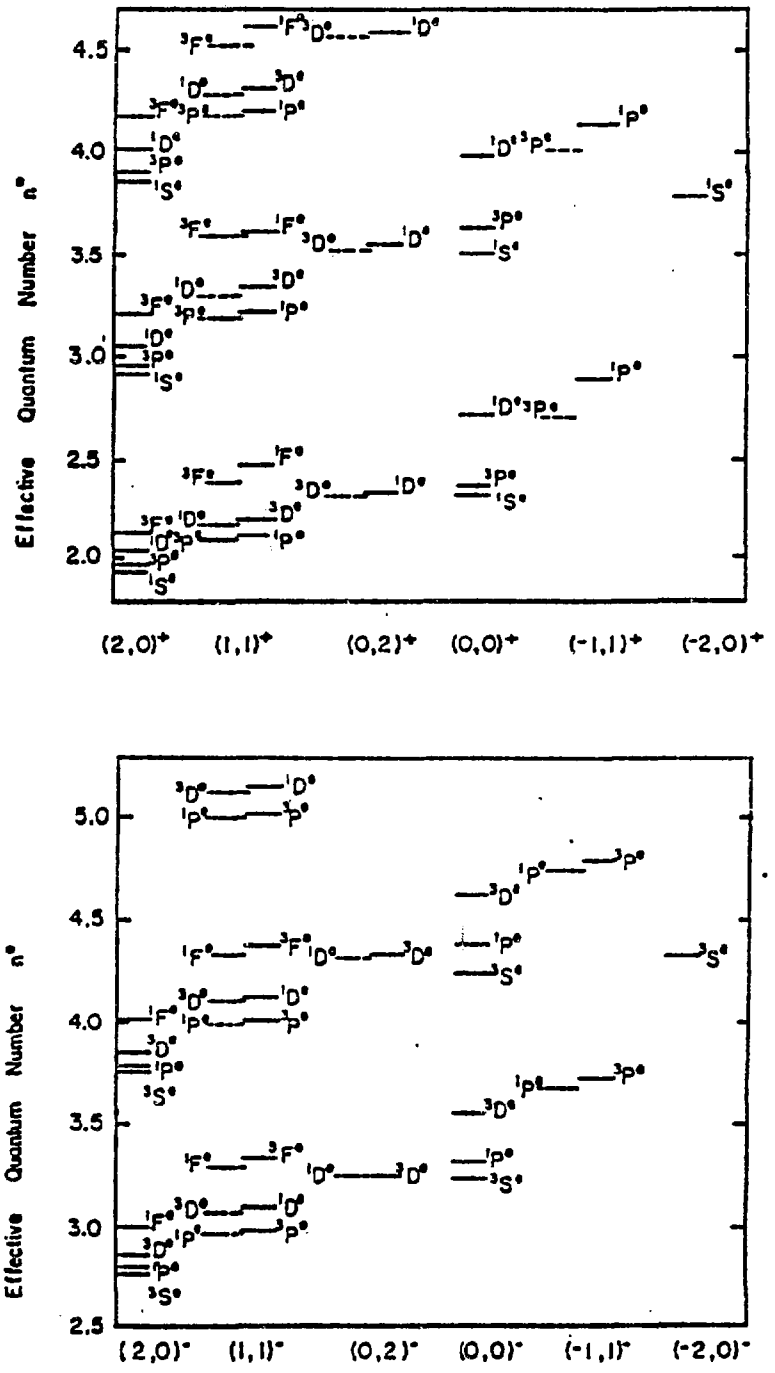

Fig. 10 Effective quantum numbers n^* grouped according to the $(K,T)^A$ scheme. The A=+1 and A=−1 groups are displayed separately. Along each column, the rotor structure is obvious. Energy levels are taken from Ref. 40.

The energy levels shown in Fig. 10 were taken from the extensive CI calculation of Lipsky et al.[40] Some of the levels shown have been reclassified to preserve the regular rotor structure shown. We also notice that for channels with $T \neq 0$, there are two series for each $(K,T)^A$, one with parity given by $(-1)^L$ and the other by $(-1)^{(L+1)}$. The energy levels of the latter group is always slightly lower than the former. This near-degeneracy is called T-doubling. The radial and angular correlations between each pair of groups are quite similar. It can be shown[41] that the wave function for each member of the group with parity $(-1)^L$ has a nonzero amplitude near $\theta_{12} = 0°$ while for members of the other groups the amplitude at $\theta_{12}=0°$ vanishes. This results in slightly different Coulomb repulsion between the two electrons.

The rotorlike structure shown above is expected only for doubly excited states which have been assigned with A=+1 and -1. States where A=0 behave like singly excited states. Their energy levels are such that for a given $(K,T)^\circ$ channel, the triplet state always lies lower than the corresponding singlet state, similar to the familiar level ordering of singly excited states of He. For more details see ref. 32.

4.5 Body-Frame Analysis Of The Channel Functions[41]

The quantum numbers assigned empirically from analyzing the channel functions in hyperspherical coordinates can be better understood by looking at the solution in the body frame of the system. Starting with a given wave function in the laboratory frame expressed in the conventional independent particle coordinates,

$$\Psi(\vec{r}_1,\vec{r}_2) = \sum_{l_1 l_2} \Psi^L_{l_1 l_2}(r_1,r_2)\ \mathcal{Y}_{l_1 l_2 LM}(\hat{r}_1,\hat{r}_2) \qquad (25)$$

one can rewrite the wave function in the body frame by invoking a rotation. Suppose that we define the body frame to be formed by the three particles, with the interelectronic axis as the z'-direction of the body frame. The transformation from the laboratory frame to the body frame is represented by a rotation matrix, $D(\hat{\omega})$,

$$\mathcal{Y}_{l_1 l_2 LM}(\hat{r}_1,\hat{r}_2) = \sum_Q \mathcal{Y}_{l_1 l_2 LQ}(\hat{r}'_1,\hat{r}'_2)\ D^{(L)}_{QM}(\hat{\omega}) \qquad (26)$$

In (26), $\hat{\omega}$ represents the Euler angles, $\hat{r}_1'$ and $\hat{r}_2'$ are the spherical angles of the two electrons in the body frame. Using (25) and (26), the wave function is expressed in the body frame by

$$\Psi(\vec{r}_1,\vec{r}_2) = \sum_Q \psi_Q^L(R,\alpha,\theta_{12}) \quad D_{QM}^{(L)}(\hat{\omega}) \tag{27}$$

where

$$\psi_Q^L(R,\alpha,\theta_{12}) = \sum_{l_1 l_2} \psi_{l_1 l_2}^L (R\cos\alpha, R\sin\alpha) \; \mathcal{Y}_{l_1 l_2 LQ}(\hat{r}_1',\hat{r}_2') \tag{28}$$

and $-L \leq Q \leq L$. Thus Q is the projection of L onto the body-frame axis. Let us consider the symmetry of the function Ψ_Q^L under particle exchange. A careful analysis shows that under $\alpha \to \frac{\pi}{2}-\alpha$, each rotational component satisfies

$$\psi_Q^L(R,\ \pi/2-\alpha,\ \theta_{12}) = \pi(-1)^{S+Q}\ \psi_Q^L(R,\alpha,\theta_{12}) \tag{29}$$

By introducing a phase factor A as

$$A = \pi(-1)^{S+T} \tag{30}$$

where $T=|Q|$, the index A determines the reflection symmetry of the radial wave function with respect to the $\alpha = \pi/4$ axis. Thus A serves as an index for radial correlation. In the special case when $L=0$, and $T=0$, $A=(-1)^S$. This is the simple symmetry requirement for singlet and triplet S states. For L not equals to zero, there are more than one rotational component in (27). If there is only one rotational component T, then T and A are good quantum numbers (they are related by eq. 30). Small admixture of different T components would then make T as an approximate quantum number which also makes A an approximate quantum number. Thus the purity of +/- radial correlation is reflected in the purity of rotational states.

To check the purity of rotational states, we show in Fig. 11 the decomposition of the $(1,1)^-\ ^3P^o$ and $(1,1)^+\ ^1P^o$ channel functions of He at the values of R where their respective potentials bottom out. The

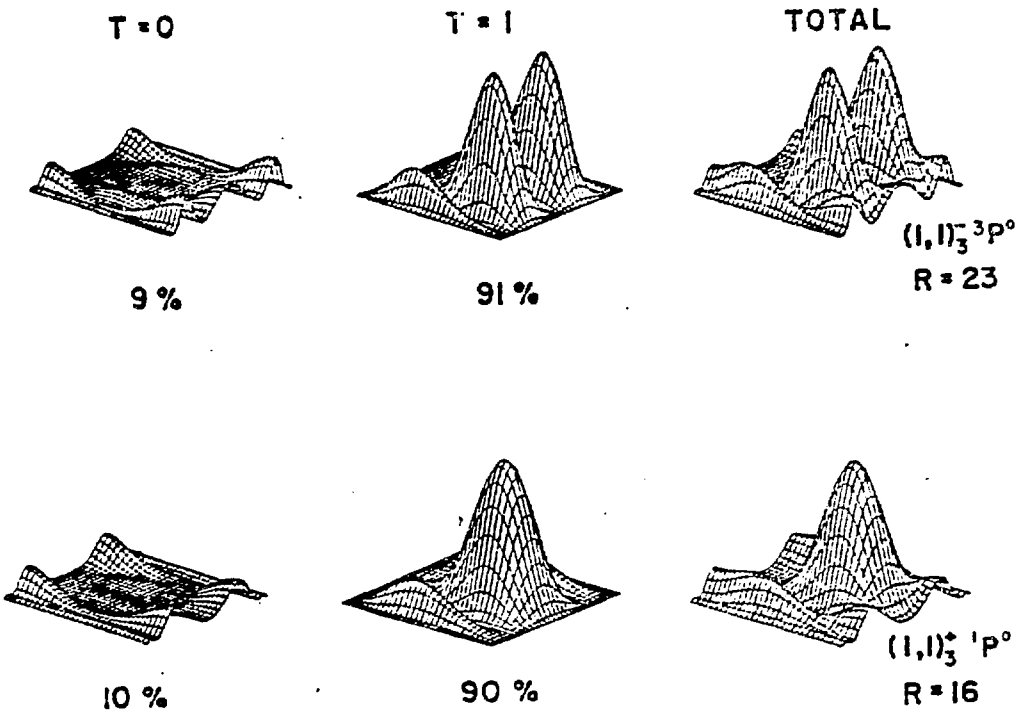

Fig. 11 Decomposition of the $(1,1)^+ {}^1P^o$ and $(1,1)^- {}^3P^o$ channels of He at the R values shown into rotational components. Percentage represents the contribution to the normalization from each T component.

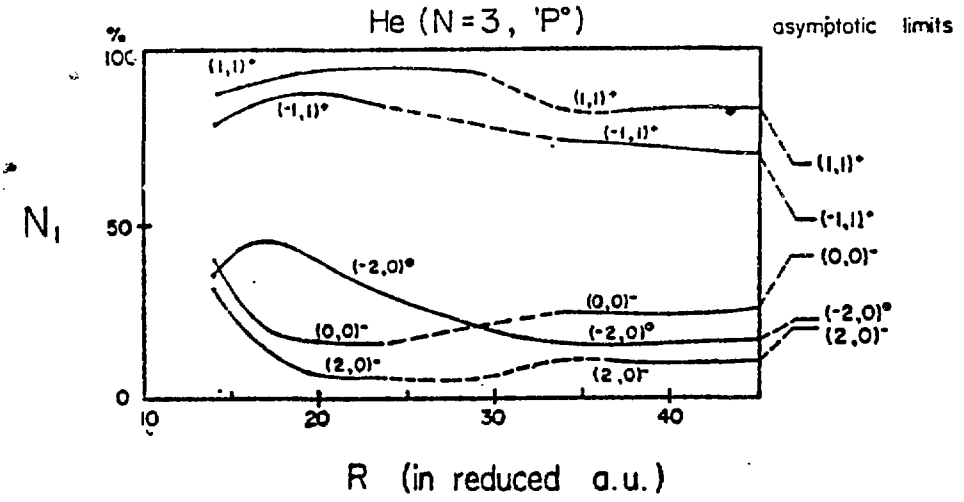

Fig. 12 The percentage of the T=1 component for all the five $^1P^o$ channels of He(N=3) as a function of the hyperradius R.

percentage represents the contribution to the normalization from each T component. For $^3P^o$, the T=1 component is 91%, while for $^1P^o$, it is 90%. According to eq. (30), the A values are +1 and -1 respectively. These A and T values are consistent with the assignment described in eq. 24. The purity of rotational states maximizes roughly in the range where the potential is near its minimum. To illustrate the dependence of the purity of the rotational states on R for each channel, in Fig. 12 we show the percentage of the T=1 component for all the five $^1P^o$ channels that converge to the He^+ (N=3) thresholds. The dashed lines represent the interpolated region where the potential curves exhibit diabatic crossings. By referring to the $(K,T)^A$ classification, we note that the purity of T is not very good for the higher channels. These channels are classified with A=0. We further note that the rotational quantum number is ill-respected in the asymptotic region.

Each rotational component wave function also exhibits symmetry with respect to the $\theta_{12}=\pi$ axis. In fact, it can be shown that[41]

$$\Psi^L_Q(R;\alpha,2\pi-\theta_{12}) = (-1)^T \Psi^L_Q(R;\alpha,\theta_{12}) \qquad (31)$$

Thus channels with T odd exhibits a nodal line at $\theta_{12} = \pi$.

The body-frame analysis does not provide information about K-quantum number. One can relate the quantum number K to the nodal structure in θ_{12}. This is understood by looking at the wave function in the asymptotic region. Take the axis of the approaching electron to be the z-axis of the laboratory frame. In this frame the two electron wave function is $P^Q_{l_2}(\cos\theta_{12})$ where $Q=\vec{L}.\hat{r}_1$. The number of nodes in θ_{12} $(0 < \theta_{12} < \pi)$ is $l_2-|Q|$ which varies between 0 and N-1-T. The transformation from the laboratory to the body frame is identity at large r_1. Thus for a given T, we can use the number of nodes in θ_{12} to label the vibrational motion in θ_{12}. The vibrational quantum number v is related to the number of nodes n by

$$v=2n+T \qquad (32)$$

The quantum number K used for labeling hyperspherical channels is related to n and v by

$$K=N-2n-T-1 \qquad (33)$$
$$=N-v-1$$

From Fig. 11 we can see the number of nodes in θ_{12} is consistent with the equation above. Since the angular correlation does not vary significantly with R, this analysis in the asymptotical region is valid also in the inner region.

To summarize this section, we point out that the analysis of the channel functions in hyperspherical coordinates allows us to obtain a complete classification scheme for all doubly excited states. The new correlation quantum numbers K and T provide information on the vibrational and rotational motions of the two correlated electrons, while the radial correlation quantum number A provides the in-and-out stretching of their radial motion. In terms of these quantum numbers, new spectroscopic regularities can be easily established. The supermultiplet structure is a consequence of the heirachial order of the rotational (U_T), the vibrational (U_K), and the stretching (U_A) energies which follow the approximate order

$$U_A >> U_K >> U_T \qquad (34)$$

There are other schemes of ordering doubly excited states. By ordering states with increasing number of vibrational nodes, a d-supermultiplet structure[38] with the shape of a diamond can be obtained. Such a structure exists for the + as well as for the - states.[41]

Other aspects like T-doubling and the systematic of widths will not be discussed here but can be easily anticipated or interpreted in hyperspherical coordinates. The reader is referred to Ref. 41. We conclude this section by pointing out that hyperspherical coordinates do provide a systematic method for the analysis of internal motions of two-electron atoms and for a new classification scheme of doubly excited states.

5. VIBRATIONAL MODES OF LINEAR TRIATOMIC MOLECULES AND DIAMAGNETISM OF ATOMIC HYDROGEN

The quasi-separable approximation in hyperspherical coordinates

has been used in several other areas. In this section, we give two other examples: (1) Hyperspherical modes for a linear triatomic molecule and; (2) quadratic Zeeman effect.

5.1 Hyperspherical Modes Of Linear Triatomic Molecules[4]

An example of model potential used by quantum chemists for a linear ABA molecule was given in Fig. 3. By using a separable approximation,[42] a normalized wave function is expressed as

$$\Psi_{v_1 v_3}(R,\alpha) = F_{v_1 v_3}(R)\ \Phi_{v_3}(R;\alpha) \tag{35}$$

where the ' channel fucntion' Φ satisfies the equation

$$\left[-\frac{\hbar^2}{2m}\ \frac{1}{R^2}\frac{\partial^2}{\partial\alpha^2} + V(R,\alpha)\right]\ \Phi_{v_3}(R;\alpha) = E_{v_3}(R)\Phi_{v_3}(R;\alpha) \tag{36}$$

The potential V is usually assumed to be of Morse-oscillator type,

$$V(r_{AB},r_{BA}) = D\ \{1-\exp[-\alpha(r_{AB}-r^{o}_{AB})]\}^2 + D\ \{1-\exp[-\alpha(r_{BA}-r^{o}_{BA})]\}^2-2D \tag{37}$$

with suitable parameters for different systems. Examples of the effective potentials $E_{v_3}(R)$ are given in Fig. 13 for the ABA system. Because there are two identical particles in the system, for each vibrational level v_3 of AB in the dissociation limit, there are two effective potential curves which converge to each v_3-limit, the lower curve corresponds to the gerade (A=+) symmetry and the upper one to the ungerade (A=-) symmetry. Because of the lack of rotational motion, the +/- symmetry in α in linear triatomic molecules is exact. Therefore, each effective potential curve or channel is labelled by a quantum number v_3 and a gerade or ungerade symmetry. By solving the vibrational energy levels for each channel each state is labelled by another vibrational quantum number v_1. Thus, each state can be designated by $(v_1, v_3)^{\pm}$ where the +/- indicates the symmetry of the total wave function with respect to the hyperangle at $\alpha = \alpha_{max}/2$.

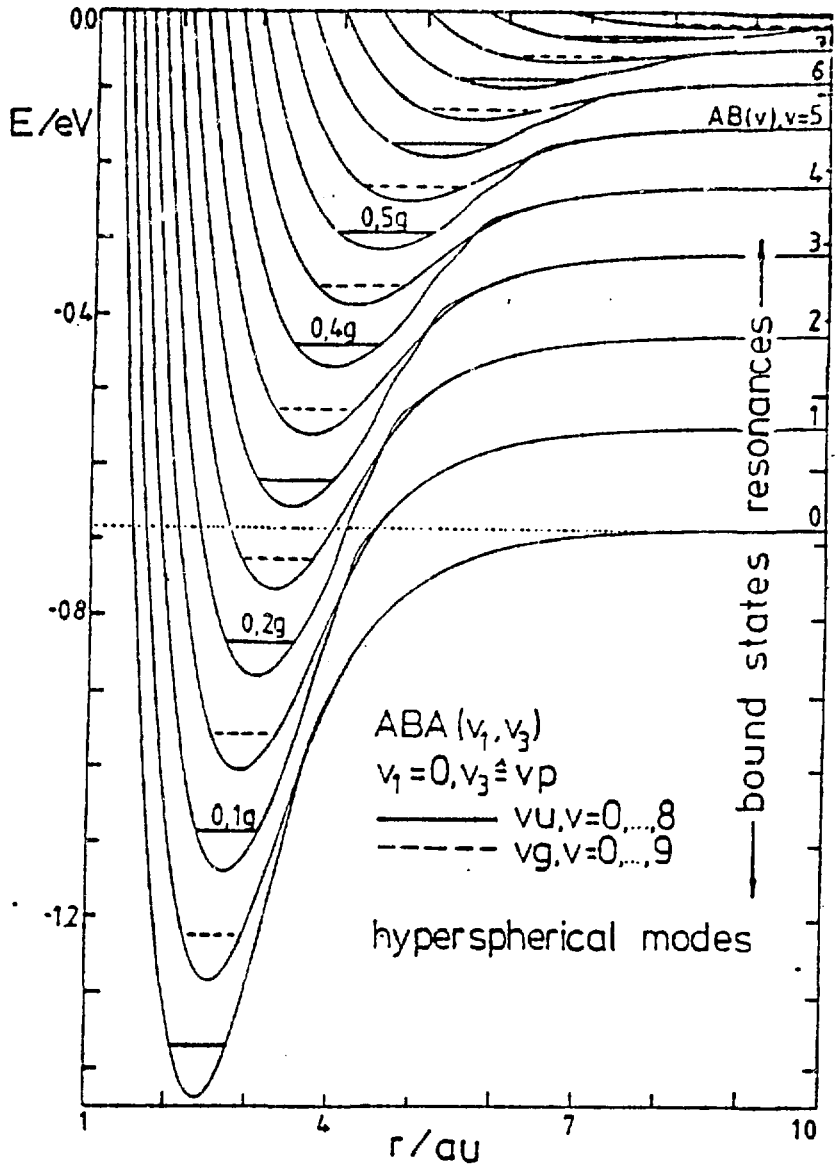

Fig. 13. Effective potential curves for a model linear triatomic ABA molecule calculated in the adiabatic approximation. (From Ref. 42.)

Each of the vibrational state $(v_1, v_3)^{\pm}$ above becomes unstable when the channel couplings are included if the state lies above the first vibrational state in the dissociation limit. These couplings can be included by solving the coupled differential equations in the hyperradial coordinate. The vibrational states calculated above are then shown as resonances. The widths of the resonances reflect the strengths of

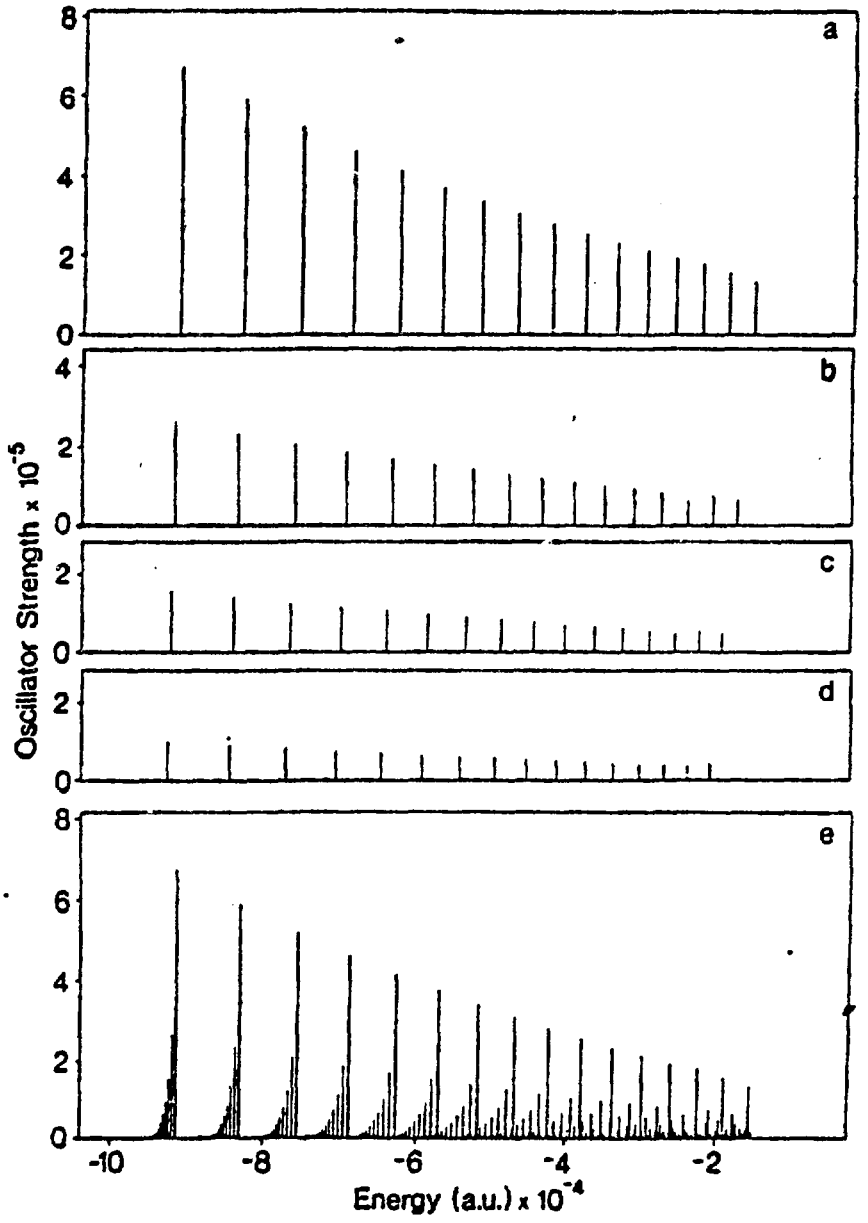

Fig. 14 The σ polarization absorption spectrum of hydrogen in a magnetic field of 47 KG. Frame (e) shows the net oscillator strength distribution in this energy range; frames (a)-(d) depict the principal, second, third and fourth series, respectively. (From Ref. 45.)

channel couplings. Model calculation for the reaction such as

$$F + H_2 \rightarrow FH + H \qquad (38)$$

has been carried out by Launay and Le Dourneuf.[43] Their results showed

that the reactive cross sections display many resonances; some of these are narrow and others are quite broad. The broad resonances are associated with + channels and the narrow ones with - channels. This situation is similar to that of the doubly excited states of He except that the model problem here is simpler and only two coordinates are used. Unlike the two-electron problems, the +/- symmetry in this problem is exact.

5.2 Quadratic Zeeman Effects In Atomic Hydrogen

As a last example, we consider the diamagnetism of atomic hydrogen. For a recent review on the subject of the effects of magnetic fields on atoms, the reader is referred to Ref. 44.

In Fig. 14 the calculated partial photoabsorption spectrum of hydrogen in a magnetic field of 47kG is shown. The light is polarized linearly perpendicular to the field axis. These results are obtained[45] by using a large basis set of Sturmian functions to diagonalize the Hamiltonian of a hydrogen atom in a magnetic field. The entire calculated spectra are shown at the bottom frame, while the principal, the second, the third and the fourth series, respectively, are displayed in frames (a)-(d). One can clearly see that the oscillator strengths, after being regrouped into series, become very smooth as a function of the total energy and the strength varies systematically from one group to the next. This difference in oscillator strength among different series can be attributed to the nodal structure of the wave function in the angular part of the 'hyperspherical coordinates'. In the present case, the hyperspherical coordinates are the usual spherical coordinates. By displaying the wave function on the angular coordinate θ (the ϕ - dependence is factored out easily), the wave functions along the turning surface for various states are shown in Fig. 15. Along the first row, the angular dependence of the wave functions for the 1st, 5th,10th and 16th states of the principal series are shown. First we note that all the functions exhibit an antinode at $\theta = \pi/2$, with no nodes anywhere. For the second, third and fourth rows, similar functions for the corresponding states for the second through fourth series are shown. One notes that each higher series is

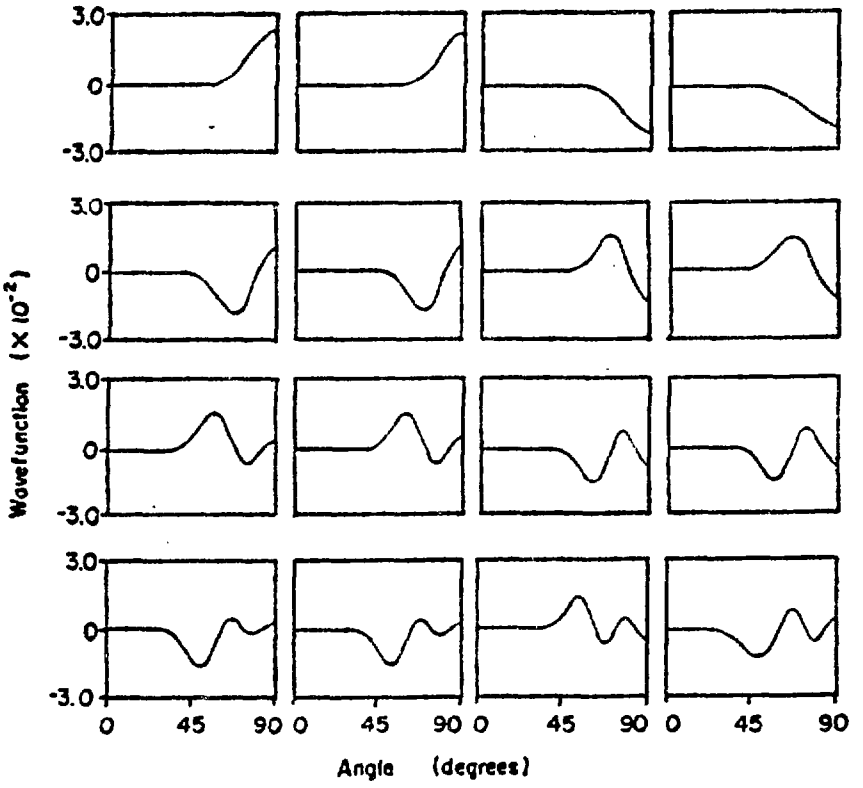

Fig. 15 Wave functions along the turning surface for various states of Fig. 14. (From Ref. 44.)

characterized by an additional node in the angle θ. Thus each series is distinguished by the number of angular nodes.

By comparing with the potential surface in Fig. 4, we also note that the functions displayed in Fig. 15 show large amplitudes near the potential ridge. Because only σ polarization is considered in Fig. 14, all the functions shown are symmetric with respect to $\theta = \pi/2$, i.e., they are all + states.

It should be mentioned that the wave functions displayed in Fig. 15 are along the classical turning surface. Such a surface is the locus of the equation

$$-\frac{1}{r} + \frac{1}{2}\beta^2 r^2 \sin^2\theta = \varepsilon \qquad (39)$$

where ε is the energy of the state involved.

VI. SUMMARY AND FUTURE PERSPECTIVE

In this article we gave a few examples of the applications of hyperspherical coordinates to atomic and molecular problems. We emphasized that the potential surfaces of a large class of problems, when expressed in hyperspherical coordinates, exhibit valleys and potential ridges. The potential ridges play an important role in determining the physical characteristics of resonance states.[23] The symmetry of the wave function along the coordinate perpendicular to the potential ridge, that whether it has + or has - character, largely determines whether the state is to be excited or not. Our documentation in this article emphasizes doubly excited states of two-electron atoms as well as simple two-dimensional problems from model linear triatomic molecules and diamagnetic effects in hydrogen.

In the last few years we have witnessed the success of applying hyperspherical coordinates to many problems in atomic and molecular physics, particularly in the understanding of resonances. This field is just in its infancy. Progress will be accelerated as better computational methods are developed. Extension of hyperspherical coordinates to two-valence-electron atomic systems have been applied by several workers[46-49] where a similar classification scheme as for two-electron atoms has been established.[49] Extension of the method to the situation where both electrons are highly excited is also in its beginning.[50] There are the threshold electron impact ionization studies under the umbrella of "Wannier theory" where hyperspherical coordinates are the base of most investigations. There are also some initial application of hyperspherical coordinates to three-electron atoms[51] and some analysis of hyperspherical harmonics in the N-electron atomic systems.[52] All of these investigations are still in the very early stage.

In the area of quantum chemistry, the application of hyperspherical coordinates in the last few years had also been quite fruitful.[53,54] Most of these studies are confined to model problems. It has been shown that the different vibrational modes are better explained using hyperspherical coordinates than traditional coordinates. Applications of hyperspherical coordinates to reactive scatterings in collinear systems have also shown that the rearrangement

reaction is more conveniently formulated in hyperspherical coordinates. Extension of the method to real three-dimensional collisions will be desirable in the future.

There are few applications of hyperspherical coordinates to electron atom scatterings so far. In describing resonances as well as the situation when the particles are close together hyperspherical coordinates are superior to independent particle coordinates. In scattering problems, the problem in the asymptotic region is better formulated in terms of the independent particle picture. To treat the whole scattering problem, it is necessary to develop propagation or matching methods that transform the solution from one region using one coordinate system to that in another region using another coordinate system. Preliminary studies[55] along these lines are being developed and progress can be expected in the near future. Progress in this area will also allow us to forsee a unified treatment of electron-atom scatterings and reactive scatterings.

Acknowledgement

Partial support for the work reported here has been provided by the U.S. Department of Energy, Division of Chemical Sciences.

References

1. U. Fano, Rep. Prog. Phys. 46, 97 (1983), and references therein.
2. C.D. Lin, in Adv. Atomic and Mole. Physics (1986).
3. See A.R.P. Rau in Atomic Physics 9, edited by R.S. Van Dyck, and E.N. Fortson, World Scientific Pub. Co. (1984).
4. J. Manz, Comments At. Mol. Phys. 1985.
5. D.R. Herrick, this volume.
6. W. Smith, this volume.
7. T.H. Gronwall, Phys. Rev. 51, 655 (1937); J.H. Bartlett, Jr., Phys. Rev. 51, 661 (1937).
8. V. Fock, Det. Kong. Norske Vidensk. Selsk. Forhandl. 31, 138, 145 (1958).
9. K. Frankowski and C.L. Pekeris, Phys. Rev. 46, 146 (1966).
10. G.H. Wannier, Phys. Rev. 90, 817 (1953).
11. R.P. Madden and K. Codling, Phys. Rev. Lett. 10, 516 (1963).
12. J.W. Cooper, U. Fano and F. Prats, Phys. Rev. Lett. 10, 518 (1963).
13. J.H. Macek, J. Phys. B1, 831 (1968).
14. (a) C.D. Lin, Phys. Rev. A10, 1986 (1974); (b) ibid. 12, 493 (1975).
15. A.R.P. Rau, Phys. Rev. A4, 207 (1971); C.H. Greene and A.R.P. Rau. Phys. Rev. Lett. 48, 533 (1982).
16. R. Peterkop, J. Phys. B4, 513 (1971).
17. H. Klar and W. Schlecht, J. Phys. B: Atom. Molec. Phys. 9, 1699 (1976); H. Klar, Phys. Rev. A15, 1452 (1977); H. Klar and M. Klar, Phys. Rev. A17, 1007 (1978); J. Phys. B: Atom. Molec. Phys. 13, 1057 (1980).
18. L.M. Delves, Nucl, Phys. 9, 391 (1958/59); 20, 275 (1960) W. Zickendraht, Ann. Phys. (N.Y.) 35, 18 (1965).
19. T.G. Winter and C.D. Lin, Phys. Rev. A29 3071 (1984).
20. C.H. Greene, Phys. Rev. A26, 2974 (1982).
21. J. Manz and J. Romelt, Chem. Phys. Lett. 81, 1979 (1981).
22. See the review by R.H. Garstang, Rep. Prog. Phys. 40, 105 (1977).
23. U. Fano, Phys. Rev. A24, 2402 (1981).

24. (a) D.L. Knirk, J. Chem. Phys. 60, 66 (1974); (b) ibid, 60, 760 (1974); (c) Phys. Rev. Lett. 32, 651 (1974).
25. K.K. Fang, J.S. Levinger and M. Fabre de la Ripelle, Phys. Rev. C17, 24 (1978); K.K. Fang, Phys. Rev. C19, 1637 (1979).
26. B.L. Christensen-Dalsgaard, Phys. Rev. A29, 470 (1984).
27. C.D. Lin, Phys. Rev. A23, 1585 (1981).
28. C.D. Lin, Phys. Rev. Lett. 35, 1150 (1975).
29. See G.J. Schulz, Rev. Mod. Phys. 49, 378 (1973); J.S. Risley, in Atomic Physics 4, edited by G. Zu. Putlitz, E.B. Weber, and A. Winnacker (Plenum, New York, 1975).
30. H.C. Bryant, B.D. Dieterle, J. Donahue, H. Sharifian, H. Tootoonchi, D.M. Wolfe, P.A.M. Gram and M.A. Yates-Williams, Phys. Rev. Lett. 38, 228 (1977).
31. C.D. Lin, Phys. Rev. Lett. 51, 1348 (1983).
32. C.D. Lin, Phys. Rev. A29, 1019 (1984).
33. I.C. Percival and M.J. Seaton, Proc. Cambridge Philos. Soc. 53, 654 (1957).
34. D.R. Herrick, Phys. Rev. A12, 413 (1975).
35. C.D. Lin, Phys. Rev. A15, 1535 (1982).
36. D.R. Herrick and O. Sinanoglu, Phys. Rev. A11, 97 (1975).
37. A.R.P. Rau. private communication.
38. (a) M.E. Kellman and D.R. Herrick, Phys. Rev. A22, 1536 (1980); J. Phys. B11, L755 (1978), (b) D.R. Herrick, M.E. Kellman, and R.D. Poliak, Phys. Rev. A22, 1517 (1980), (c) D.R. Herrick, Adv. Chem. Phys., 52, 1 (1983).
39. (a) P. Rehmus and R.S. Berry, Chem. Phys., 38, 257 (1979), (b) G.S. Ezra and R.S. Berry, Phys. Rev. A25, 1513 (1982).
40. L. Lipsky, R. Anania, and M.J. Corneely, Atomic Data and Nuclear Data Tables 20, 727 (1977).
41. S. Watanabe and C.D. Lin, Phys. Rev. (1985) submitted.
42. J. Manz and H.H.R. Schor, Chem. Phys. Lett. 107, 542 (1984).
43. J.M. Launay and M. Le Dourneuf, J. Phys. B: Atom. Molec. Phys. 15, L455 (1982).

44. C.W. Clark, K.T. Lu, and A.F. Starace, in Progress in Atomic Spectroscopy, part C. Edited by H.J. Beyer and H. Kleinpoppen (Plenum Pub. Corp. 1984).
45. C.W. Clark and K.T. Talor, J. Phys. Rev. B13, L737 (1980).
46. C.H. Greene, Phys. Rev. A23, 661 (1981).
47. C.D. Lin, J. Phys. B16, 723 (1983).
48. S. Watanabe, Phys. Rev. A25, 2074 (1982).
49. M. Le Dourneuf and S. Watanabe, to be published (1985).
50. C.D. Lin, Phys. Rev. A26, 2305 (1982).
51. C.H. Greene and C.W. Clark, Phys. Rev. A30, 2161 (1984); C.W. Clark and C.H. Greene, Phys. Rev. A21, 1786 (1980); S. Watanabe, M. Le Dourneuf and L. Pelamourgues, Colloque International 334 du Centre National de la Recherche Scientifique [J. Phys. (Paris) Suppl. 43, 223 (1982)].
52. M. Cavagnero, Phys. Rev. A30, 1169 (1984).
53. M. Tamir, U. Halavee and R.D. Levine, Chem. Phys. Lett. 25, 38 (1974).
54. A. Kuppermann, Chem. Phys. Lett. 32, 374 (1975).
55. B.L. Christensen-Dalsgaard, Phys. Rev. A29, 470, 2242 (1984).
56. J.T. Broad and W.P. Reinhardt, Phys. Rev. A14, 2159 (1976).
57. J. Manz and J. Römelt, Chem. Phys. Lett. 81, 179 (1981).